




Thermal mechanism-driven microlens formation in Ge–Sb–S glasses by direct laser writing: composition dependent insight

J. Smolík^{1,2}, P. Knotek^{3,*} , E. Černošková^{2,3}, P. Kutálek^{1,2}, E. Samsonova³, J. Schwarz³, J. Kašparová⁴, and L. Tichý³

¹ Center of Materials and Nanotechnologies, Faculty of Chemical Technology, University of Pardubice, Cs. Legii 565, 530 02 Pardubice, Czech Republic

² Joint Laboratory of Solid State Chemistry, Faculty of Chemical Technology, University of Pardubice, Studentská 84, 532 10 Pardubice, Czech Republic

³ Department of General and Inorganic Chemistry, Faculty of Chemical Technology, University of Pardubice, Studentská 573, 532 10 Pardubice, Czech Republic

⁴ Faculty of Chemical Technology, Institute of Applied Physics and Mathematics, University of Pardubice, Studentská 95, 532 10 Pardubice, Czech Republic

Received: 22 October 2023

Accepted: 4 January 2024

Published online:
10 February 2024

© The Author(s), 2024

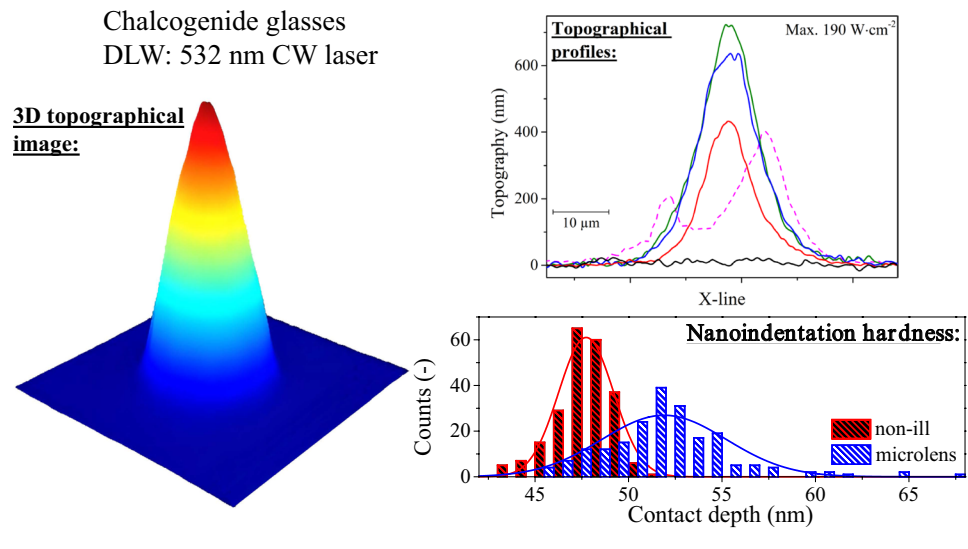
ABSTRACT

Microlenses were fabricated through a thermal process using laser-induced localized overheating on the surfaces of various bulk Ge–Sb–S glasses. These glasses spanned three distinct groups: (a) stoichiometric $(\text{GeS}_2)_{1-x}(\text{Sb}_2\text{S}_3)_x$ glasses with $x = 0\text{--}0.88$; (b) a series with a constant Sb content represented as $\text{Ge}_x\text{Sb}_{0.17}\text{S}_{0.83-x}$ $x = 0.13\text{--}0.24$, and (c) glasses with a constant Ge content denoted by $\text{Ge}_{0.18}\text{Sb}_x\text{S}_{0.82-x}$ $x = 0.03\text{--}0.10$. A continuous-wave laser emitting at 532 nm was used in the fabrication process. Both the photo-induced microlenses and the non-illuminated surfaces underwent characterization to determine their topography (via digital holographic microscopy), chemical composition (using EDX analysis), structure (through Raman spectroscopy), and mechanical properties (assessed by Nanoindentation). The influence of the chemical composition was studied to identify parameters that described the characteristics of the formed microlenses, such as the maximum achieved height and the threshold power density for microlens formation. For $(\text{GeS}_2)_{0.66}(\text{Sb}_2\text{S}_3)_{0.34}$ glass, the effective focal length of the produced microlenses was calculated to be approximately 145–190 μm , potentially aiding in the miniaturization of optical devices that, in the context of Ge–Sb–S, working primarily in the near and/or mid-IR region.

Handling Editor: Andréa de Camargo.

Address correspondence to E-mail: petr.knotek@upce.cz

GRAPHICAL ABSTRACT



Introduction

Laser-based micromachining is a valuable technique that facilitates the miniaturization and alteration of materials at the microscale [1]. This approach can be employed to produce a variety of components applicable in fields such as micro-optics, micro-electronics, and micro-biology, as well as industries focused on renewable energy, automotive, aerospace, and more [1, 2]. Surface microstructuring is a progressive branch of materials engineering. Due to the efforts made, various routes for the formation of microlenses on the surface of glasses have been discovered with application to image processing and optical fiber bonding. As an alternative route to the presented direct laser writing, surfaces are modified employing hot-embossing by heating the surface through a stamp, e.g. [3, 4], additive printing technology of optical material with lower resolution and limit in optical quality, e.g. [5], self-assembly of microparticles on the surface, e.g. [6] or by multi-step soft lithography and wet etching techniques, see e.g. [7]. The direct laser writing (DLW) method offers several benefits over other micromachining/microstructuring techniques. These advantages include (a) non-contact modification, with no contamination of the material surface, (b) a one-step, environmentally friendly process, offering an alternative to methods like chemical etching, and (c) the ability to modify materials by selectively removing different

compounds through varied laser illumination durations, wavelengths, and/or power densities [2].

Chalcogenide glasses have several advantages that make them suitable for micromachining/microstructuring using DLW. (a) They can be prepared in multiple forms, including bulk samples, thin films, and fibers, offering flexibility for diverse applications. (b) These glasses exhibit high infrared transparency, higher values of linear and nonlinear refractive indexes, and comparably low glass transition temperatures, melting temperatures, and bond energies. This makes them ideal for various optical, optoelectronic, and electrical devices operating in the near and mid-IR regions [8, 9]. (c) Chalcogenide glasses are also often photo-sensitive, aiding in localized surface modifications using the DLW technique, e.g. photo-induced volume changes like photo-expansion [10, 11], photo-contraction [12, 13] or ablation [14, 15], commonly used in glassy surface microstructuring and forming concave or convex microlenses and their arrays [13, 16–18].

Ge–Sb–S glasses are well-established glassy systems. Consequently, several of their attributes, including glass-forming ability [19–21], density [22–24], structure, e.g. [25–29], optical [22, 30, 31], thermal [22–24, 30, 32], electrical [24, 30] or mechanical [22] properties, have been investigated. Additionally, this glassy system is devoid of any toxic elements at low concentrations. Yet, only a limited number of studies have explored the photo-induced surface

alterations, with particular attention to some chemical compositions from the Ge–Sb–S glassy system. These include: (a) Formation of microlenses on the surface of $(\text{GeS}_2)_{0.74}(\text{Sb}_2\text{S}_3)_{0.26}$ when illuminated by a CW 532 nm laser, attributable to the local thermal expansion of the overheated material [33]. (b) Formation of smooth microcraters due to increased viscous flow, as well as microcraters surrounded by a notable number of ejected particles because of explosive boiling, both observed on the surface of bulk glassy $\text{Ge}_{0.35}\text{Sb}_{0.10}\text{S}_{0.55}$ using a CW laser emitting at 785 nm [34]. (c) Formation of microcraters on the bulk samples and thin films through ablation under pulsed laser illumination ($(\text{GeS}_2)_{0.3}(\text{Sb}_2\text{S}_3)_{0.7}$, illuminated by a 5 ns pulsed laser emitting at 213 nm) [35].

The objective of this study is to investigate the formation of microlenses on the surface of Ge–Sb–S bulk glasses using a CW laser emitting at 532 nm. Additionally, the research evaluates how chemical composition affects the characteristics and properties of the resulting microobjects/lenses. The chemical compositions studied include a stoichiometric set of glasses represented by $(\text{GeS}_2)_{1-x}(\text{Sb}_2\text{S}_3)_x$ ($x = 0–0.88$), and two sets of samples with a constant amount of either Ge or Sb, represented as $\text{Ge}_x\text{Sb}_{0.17}\text{S}_{0.83-x}$, where $x = 0.13–0.24$, and $\text{Ge}_{0.18}\text{Sb}_x\text{S}_{0.82-x}$, with $x = 0.03–0.10$.

The created microlenses have been analyzed in terms of key parameters crucial for potential applications, such as fundamental dimensions and focal length. Given the variations in the chemical composition of the glasses studied, the continuous-wave laser emitting at 532 nm enables an examination of the influence of over-band gap, near-band gap, and sub-band gap photons on microlens formation.

Experimental

Three sets of bulk glasses of Ge–Sb–S system were prepared, i.e. (a) stoichiometric compositions $(\text{GeS}_2)_{1-x}(\text{Sb}_2\text{S}_3)_x$, $x = 0–0.88$; (b) set with constant amount of Sb: $\text{Ge}_x\text{Sb}_{0.17}\text{S}_{0.83-x}$, $x = 0.13–0.24$; and (c) glasses with constant Ge amount: $\text{Ge}_{0.18}\text{Sb}_x\text{S}_{0.82-x}$, $x = 0.03–0.10$.

The compositions we prepared and examined are based on the glass-forming ability of Ge–Sb–S glasses as per Ref. [21] and are depicted in the part of ternary Ge–Sb–S diagram in Fig. 1. The black star in Fig. 1 signifies the composition $(\text{GeS}_2)_{0.66}(\text{Sb}_2\text{S}_3)_{0.34}$, approximately $\text{Ge}_{0.18}\text{Sb}_{0.18}\text{S}_{0.64}$. This composition is

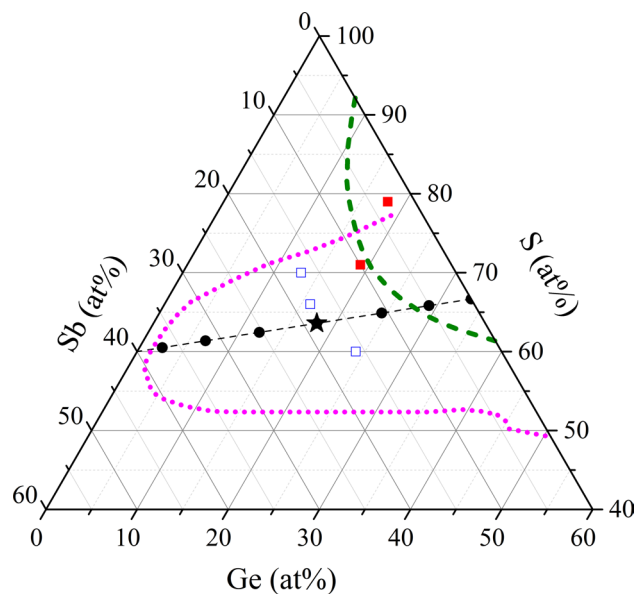


Figure 1 The part of ternary diagram Ge–Sb–S showing the chemical compositions of the prepared glasses: black circles represent the stoichiometric set $(\text{GeS}_2)_{1-x}(\text{Sb}_2\text{S}_3)_x$, $x = 0–0.88$, blue empty cubes correspond to the set $\text{Ge}_x\text{Sb}_{0.17}\text{S}_{0.83-x}$, $x = 0.13–0.24$, and red solid cubes signify the set $\text{Ge}_{0.18}\text{Sb}_x\text{S}_{0.82-x}$, $x = 0.03–0.10$. The black star indicates the composition $(\text{GeS}_2)_{0.66}(\text{Sb}_2\text{S}_3)_{0.34}$, i.e. $\approx \text{Ge}_{0.18}\text{Sb}_{0.18}\text{S}_{0.64}$, which is consistent across all three analyzed sets. The drawn dotted (magenta) and dashed (olive) lines illustrate the glass forming regions according to Ref. [21].

consistent across all three glass sets we studied. We synthesized each glass from pure elements: Ge (5N, Alfa Aesar, Germany), Sb (5N, VHG Labs, United Kingdom), and S (> 4N, Sigma-Aldrich, USA), utilizing the traditional melt-quenching method in a sealed, evacuated quartz ampoule. The mixture, with a weight aligned to the elemental ratios (around 10 g total), was placed in a rocking electric furnace. It was gradually heated up to a final reaction temperature of 950 °C. Once the melt reached this reaction temperature, we maintained its homogenization for 2 h. The resulting glass was then procured by cooling the ampoule in water. To eliminate internal stresses in the glasses post-synthesis, we annealed them at temperatures roughly 50 °C below their respective glass transition temperatures.

The samples for all optical measurements were prepared to a thickness of approximately 1.4 mm, with both surfaces polished to optical standards. For the final polishing, we used a suspension of Al_2O_3 with a grain size of 50 nm in ethylene glycol, resulting in a

Root Mean Square of Residual Roughness (RMS-RR) [36] of about 4–5 nm.

The crystalline phase’s absence in the prepared glasses was confirmed through Powder X-ray Diffraction Analysis using a D8-Advance diffractometer (Bruker AXE, Germany) equipped with Bragg–Brentano θ – θ geometry (40 kV, 30 mA), Cu K α radiation, and a secondary graphite monochromator. The real chemical composition of the glasses and the formed microlenses was verified with a JSM 5500-LV (Jeol, Japan) featuring an energy-dispersive X-ray (EDX) analysis detector (GRESHAM Sirius 10, Japan) and an accelerating voltage of 20 kV. The X-ray characteristic photons formation depth varies between \approx 2.1 and 3.2 μ m, depending on the chemical composition. EDX analysis was performed using the value of spot size parameter $<$ 50 with magnification 4000 \times for a maximum time 3 min to avoid the possible changes of materials/microlenses by the action of primary electrons. Optical properties were assessed using UV/Vis Spectroscopy with a Perkin-Elmer Lambda 12 instrument (USA). The glass transition temperature (T_g) for the examined glasses (in powder form) was determined using a Differential Scanning Calorimeter Diamond (Perkin-Elmer, USA), applying a heating rate of 10 $^{\circ}$ C min $^{-1}$ within a 50–500 $^{\circ}$ C temperature range. The coefficient of thermal expansion (CTE) below T_g was determined using rectangular bulk samples (typically 10 \times 5 \times 2 mm 3) at a heating rate of 10 $^{\circ}$ C min $^{-1}$, measured with a Thermomechanical Analysis (TMA CX 04R, R.M.I, Czech Republic). The thermal conductivity of selected samples (κ) was obtained by measuring heat capacity c_p and thermal diffusivity k using a laser flash system LFA 457 (Netzsch, Germany), for more information on the determination of κ see e.g. Ref. [37]. Microlenses were created by exposing the sample surfaces to a continuous-wave laser at λ = 532 nm. The illumination set-up was equipped with a microscope objective (60 \times magnification, 0.85 numerical aperture) producing a laser beam diameter of approximately 40 μ m and a maximum power density of 190 W cm $^{-2}$, for an exposure time of 600 s. Raman spectra of the glasses and the formed microlenses were recorded using the Raman Spectrometer Dimension-P2 (Lambda Solution, USA) with an emission at 785 nm. The reduced Raman spectra were derived from the Gammon-Shuker equation [38]. The topography of non-illuminated glassy surfaces and created micro-objects was assessed using a Digital Holographic Microscope DHMR1000 (Lynceé Tec, Switzerland)

operating at 785 nm in reflection mode. Nanoindentation measurements were conducted using the TI 950 TriboIndenter (Hysitron, Netherlands) equipped with a Berkovich-type diamond tip (maximum force: 300 μ N).

Results and discussion

Characterization of examined glasses

No traces of crystalline phases were detected in the examined glasses by XRD analysis within its detection limit. Table 1 presents the actual chemical composition of the prepared glasses. It also displays the energy values (E^{03}) corresponding to an absorption coefficient (α) of 1000 cm $^{-1}$, used here as the optical band gap width. Additionally, the table lists the optical penetration depths (d_p) for excitation light (λ = 532 nm), calculated as $d_p^{532\text{ nm}} = 1/\alpha^{532\text{ nm}}$ [33], as well as the glass transition temperature values (T_g).

From Table 1, it can be observed that the values of both E^{03} and $d_p^{532\text{ nm}}$ decrease as the Sb $_2$ S $_3$ content in stoichiometric (GeS $_2$) $_{1-x}$ (Sb $_2$ S $_3$) $_x$ increases aligning well with the findings in Refs. [22, 30]. For non-stoichiometric compositions, the values of both parameters

Table 1 List of the essential optical (expressed as optical band gap E^{03} value and optical penetration depths at λ = 532 nm, i.e. $E^{ph} = 2.33$ eV ($d_p^{532\text{ nm}}$)) and thermal properties (glass transition temperature, T_g) of the evaluated Ge–Sb–S glasses: ●—stoichiometric set (GeS $_2$) $_{1-x}$ (Sb $_2$ S $_3$) $_x$, x = 0–0.88, □—set Ge $_x$ Sb $_{0.17}$ S $_{0.83-x}$, x = 0.13–0.24, and ■—Ge $_{0.18}$ Sb $_x$ S $_{0.82-x}$, x = 0.03–0.10

(GeS $_2$) $_{1-x}$ (Sb $_2$ S $_3$) $_x$, x	E^{03} (eV)	$d_p^{532\text{ nm}}$ (μ m)	T_g ($^{\circ}$ C)
● 0	2.97	7580	443
● 0.08	2.86	2110	407
● 0.18	2.77	461	366
●, □, ■ 0.34	2.46	37	311
● 0.51	2.31	3	265
● 0.70	2.06	< 0.5	230
● 0.88	1.87	< 0.005	212
■ Ge $_{0.18}$ Sb $_{0.03}$ S $_{0.79}$	2.78	3840	193
■ Ge $_{0.19}$ Sb $_{0.10}$ S $_{0.71}$	2.62	549	262
□ Ge $_{0.13}$ Sb $_{0.17}$ S $_{0.70}$	2.54	159	289
□ Ge $_{0.16}$ Sb $_{0.18}$ S $_{0.66}$	2.51	115	307
□ Ge $_{0.24}$ Sb $_{0.16}$ S $_{0.60}$	1.96	< 0.1	327

The composition (GeS $_2$) $_{0.66}$ (Sb $_2$ S $_3$) $_{0.34}$, i.e. \approx Ge $_{0.18}$ Sb $_{0.18}$ S $_{0.64}$, designated by ●, □, ■ and the black star in Fig. 1, is shared across all three investigated sets

diminish with reduced sulfur content. Furthermore, $d_p^{532\text{ nm}}$ values span a broad range, from hundreds of nanometers to millimeters (see Table 1). Thus, the effect of varied $d_p^{532\text{ nm}}$ values on the material's response to illumination should be considered.

The glass transition temperature (T_g) was identified as the midpoint of the observed endothermic effect on DSC curve. It is important to highlight that the T_g value likely influences the formation of micro-objects, particularly during continuous-wave illumination. During this illumination, the conversion of absorbed light to heat and a subsequent rise in the local sample temperature have been noted, e.g. in [10, 33]. The values of T_g of stoichiometric compositions significantly decrease with Sb_2S_3 content which is in agreement with [22, 28, 30]. This decrease is attributed to the lower rigidity of the glassy network as a result of substitution of $\text{GeS}_{4/2}$ tetrahedra by $\text{SbS}_{3/2}$ trigonal pyramids [28]. In both sets of non-stoichiometric glasses, T_g values decrease with the increase in sulfur content. This is related to a weakened glassy structure, most probably due to formation of structural units with $-\text{S}-\text{S}-$ bridges like, e.g., $\text{S}_3\text{Ge}-\text{S}-\text{S}-\text{GeS}_3$, $\text{S}_2\text{Sb}-\text{S}-\text{S}-\text{GeS}_3$ units, as well as the formation of S_8 rings (see Raman spectra in Supplementary materials for more details).

Direct laser writing by CW 532 nm laser

The samples, polished to the optical quality, were illuminated by CW laser (532 nm), using various laser power densities up to 190 W cm^{-2} for 600 s. Depending

on the chemical composition of examined glasses, certain laser power densities induced localized volume expansions on the glass surface. These expansions remained in place after the laser was switched off. As a result, microlenses were formed, which remained stable under ambient conditions, as depicted in the SEM image in Fig. 2a.

The microlenses were analyzed using digital holographic microscopy to study their topography (Fig. 2b). A key metric for characterizing them was their height (h). As depicted in Fig. 2b (solid lines), for the $(\text{GeS}_2)_{0.66}(\text{Sb}_2\text{S}_3)_{0.34}$ glass, the height increases with the increasing laser power density (F_L), reaching up to 730 nm at $F_L = 105\text{ W cm}^{-2}$. This increase in height follows a linear trend on a logarithmic scale of laser power density, aligning well with the empirical relationship between h and $\ln F_L$ as mentioned in e.g. [33, 39]:

$$h = \alpha_{\text{eff}}^{-1} \cdot \ln \frac{F_L}{F_{\text{th}}}, \quad (1)$$

where α_{eff}^{-1} represents the effective optical penetration depth and F_{th} denotes the threshold power density necessary for the microlenses formation.

When the laser power density exceeds 105 W cm^{-2} , the formed microlenses start to exhibit deformation, evidenced by a reduction in their height. This reduction in height (h) results in a deviation from the linear trend in the relationship between h and $\ln F_L$. We attribute these deformations to the increased overheating of the illuminated region. Greater overheating amplifies viscous flow [40], which likely influences the

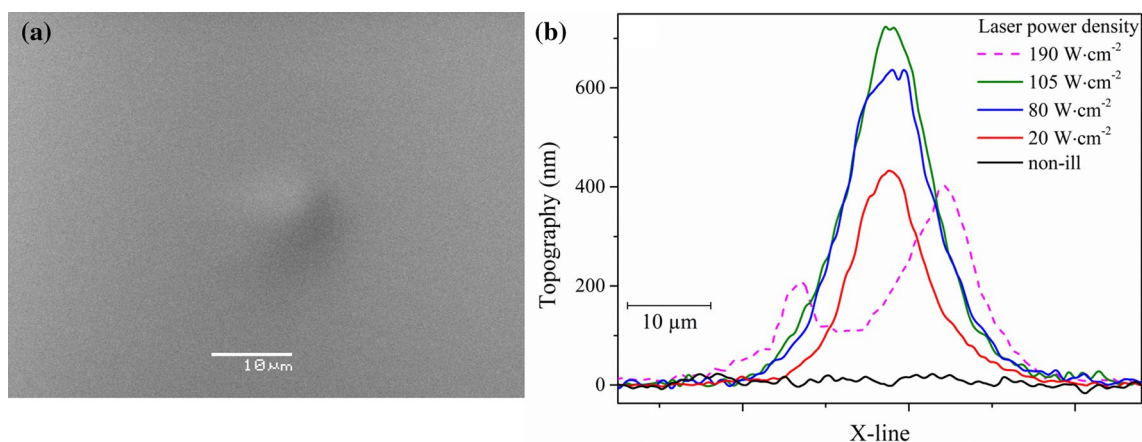


Figure 2 **a** SEM image of a microlens created on the surface of $(\text{GeS}_2)_{0.66}(\text{Sb}_2\text{S}_3)_{0.34}$ using $F_L = 105\text{ W cm}^{-2}$ for 600 s illumination and **b** the topographical profiles of microlenses

(solid line) and “dimple” deformed microlenses (dashed line, explained in the text) created on the surface of stoichiometric $(\text{GeS}_2)_{0.66}(\text{Sb}_2\text{S}_3)_{0.34}$.

changes in the height and shape of the formed microlenses. Surface tension in the molten microlenses is also expected to play a significant role. At the peak laser power density used ($F_L = 190 \text{ W cm}^{-2}$), the formerly symmetrical shape of the microlenses is altered, with a noticeable dimple forming. This altered microlens shape presents two asymmetrical peaks, probably caused by the Gaussian-like laser beam, which overheats the material most intensely at the center of the illuminated region. Additionally, an expansion in the width of the micro-object was noted.

In this text, we focus on the formation of microlenses that exhibit a regular shape consistent with the linear segment of the h versus $\ln F_L$ relationship. Several methods were employed to understand the mechanisms underlying their formation. Figure 3 displays the EDX spectra, normalized to the S-K α signal (2.307 keV). The chemical composition of the fabricated microlenses appears to be nearly identical to that of the non-illuminated surface, within experimental error margins, as shown in the results for stoichiometric $(\text{GeS}_2)_{0.66}(\text{Sb}_2\text{S}_3)_{0.34}$ (Fig. 3a) and for sulphur-rich $\text{Ge}_{0.13}\text{Sb}_{0.17}\text{S}_{0.70}$ (Fig. 3b). In addition, no deformations of microlenses and non-illuminated areas were detected by DHM after EDX analysis which confirms that the samples have not been affected by accelerating electrons during EDX analysis. Figure 4a provides typical Raman spectra for both microlens and non-illuminated samples for the two chemical compositions:

$(\text{GeS}_2)_{0.66}(\text{Sb}_2\text{S}_3)_{0.34}$ and $\text{Ge}_{0.13}\text{Sb}_{0.17}\text{S}_{0.70}$ glasses. Notably, the Raman spectra for the microlenses and the non-illuminated surfaces are virtually indistinguishable, considering the experimental error. This suggests that illumination does not induce photo-chemical changes, such as the proposed photo-oxidation believed to cause photo-expansion in Ge–Ga–S bulk glasses [41]. Similarly, no photo-structural changes were identified in either stoichiometric or non-stoichiometric glasses.

Finally, the nanoindentation hardness, as determined by the Oliver–Pharr model [42], was compared between the microlens and the non-illuminated surface. Figure 4b displays a histogram showing the contact depth to which the indenter was pressed for both the microlens and the non-illuminated $(\text{GeS}_2)_{0.66}(\text{Sb}_2\text{S}_3)_{0.34}$ glass surfaces. The indenter penetrated to a greater contact depth (h_c) on the microlens surface ($h_c = 51.9 \pm 0.2 \text{ nm}$) compared to the non-illuminated surface ($h_c = 47.7 \pm 0.1 \text{ nm}$). This increased contact depth for the microlens is associated with a 6.2 rel% reduction in nanoindentation hardness compared to the non-illuminated surface ($H_{\text{ind}} \approx 2.87 \pm 0.02 \text{ GPa}$ for the microlens and $\approx 3.06 \pm 0.01 \text{ GPa}$ for the non-illuminated surface).

Based on our findings, we hypothesize that the microlenses, i.e. local volume expansions, form on the surface of all examined glasses probably by thermal mechanism without any significant contribution

Figure 3 The comparison of EDX spectra of the highest formed microlens with non-illuminated surface (marked as non-ill) for **a** stoichiometric $(\text{GeS}_2)_{0.66}(\text{Sb}_2\text{S}_3)_{0.34}$ and **b** sulphur-rich $\text{Ge}_{0.13}\text{Sb}_{0.17}\text{S}_{0.70}$ bulk glasses.

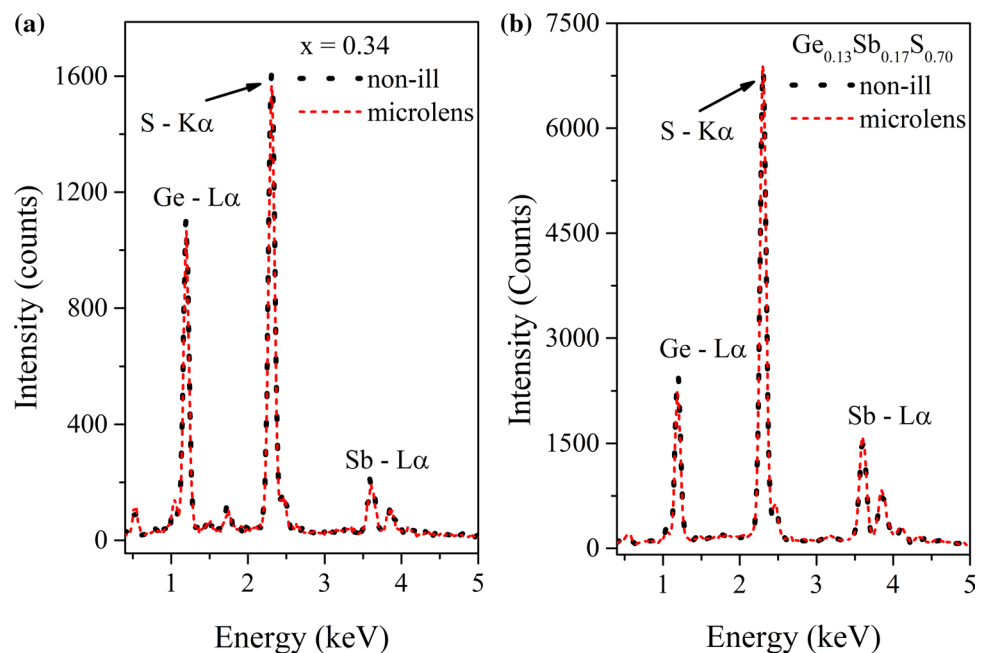
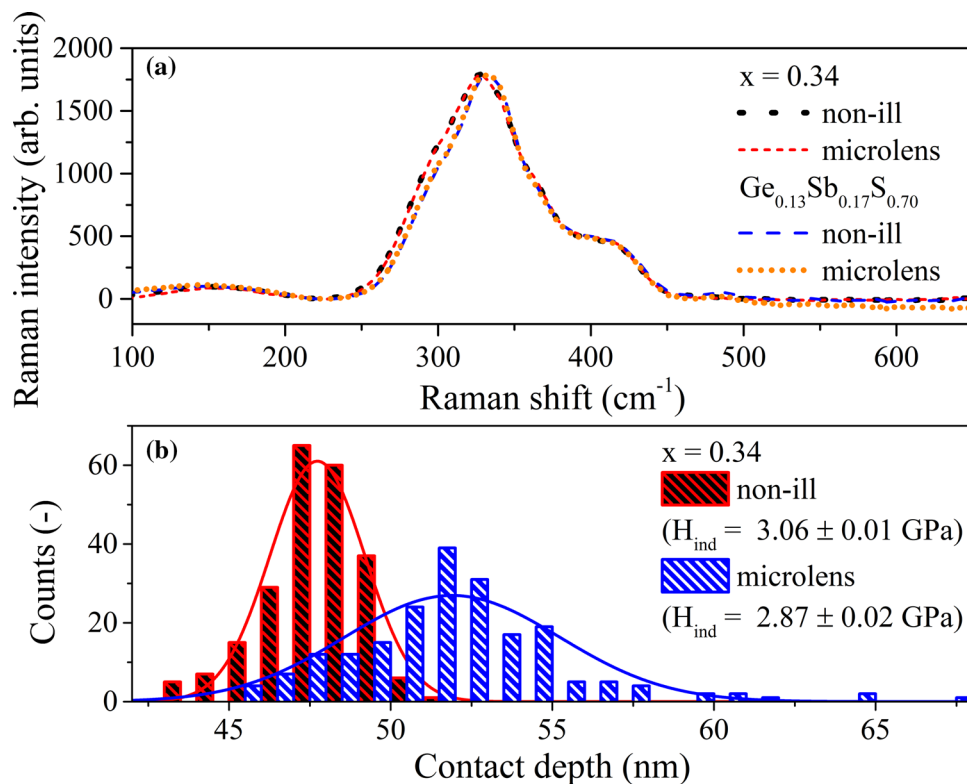


Figure 4 The comparison of **a** Raman spectra of microlens and non-illuminated surface for stoichiometric $(\text{GeS}_2)_{0.66}(\text{Sb}_2\text{S}_3)_{0.34}$ and sulphur-rich $\text{Ge}_{0.13}\text{Sb}_{0.17}\text{S}_{0.70}$ and **b** histogram illustrating the mechanical properties (contact depth, nanoindentation hardness) for microlens and non-illuminated surface of stoichiometric $(\text{GeS}_2)_{0.66}(\text{Sb}_2\text{S}_3)_{0.34}$ bulk glass, all for the highest formed microlenses.



of other factors (photo-oxidation, photo-structural changes), i.e. by a frozen-in the thermal volume expansion of locally overheated materials similarly as was observed for different chalcogenide glasses or even oxide glasses [10, 33, 43]. The stability of microlenses over time and temperature has been studied in our previous works on both Ge–Sb–S and heavy metal oxide glasses. In the case of $(\text{GeS}_2)_{0.74}(\text{Sb}_2\text{S}_3)_{0.26}$ glass [33] we observed the stability of the same microlens for 2000 h (almost 3 months) at room temperature and the height decreased in units of %. When the temperature was increased to T_g value, the microlenses disappeared and the surface was reconstructed. In the case of microlenses on $\text{PbO–Ga}_2\text{O}_3$ glasses, stability was demonstrated even after 9 months (undetectable changes in height from 1607 to 1605 nm after 9 months; see Fig. S5 in [43]). We assume that the formed microlens represents a “frozen” state, similar to rapidly cooled glass, where the rate of cooling prevents crystallization, although devitrification or macroscopic changes on topography can only occur after an extremely long time at temperatures under T_g .

Microlenses formation and the parameters characterizing microlenses shape

The parameters utilized for examining microlens formation on Ge–Sb–S glass surfaces are detailed in Table 1 and 2. Microlenses do not form on binary chalcogenide GeS_2 glass when illuminated at 532 nm, an expected outcome given that the photon energy of the employed light ($E^{\text{ph}} = 2.33$ eV) is substantially below the E^{03} value, as shown in Table 1. Under these conditions, an insufficient number of photons are captured within the sample, the absorbed energy being insufficient to trigger the glass’s photo-expansion.

On the other hand, microlenses formation was successfully induced on the surface of the other sample sets, where E^{03} ranges 1.87–2.86 eV (Table 1) covering illumination by over-band gap ($E^{\text{ph}} > E^{03}$, i.e. 2.33 eV $> E^{03}$), band-gap ($E^{03} \approx 2.33$ eV) and sub-band gap photons ($E^{\text{ph}} < E^{03}$, i.e. $E^{03} > 2.33$ eV).

For the characterization of microlens formation, we utilize the maximum height achieved by the microlenses (h_{max}) at a given laser power density ($F_{\text{max}h}$) and the threshold power density required for microlens formation (F_{th}), see Table 2. Table 2 also presents the

Table 2 Parameters used for assessing the role of chemical composition in microlenses formation for Ge–Sb–S bulk glasses: coordination number ($\langle CN \rangle$) and optical band gap (E^{03}), threshold power density needed for the microlenses formation (F_{th}), maximal obtained microlenses height (h_{max}), and the laser power density used for the obtaining h_{max} ($F_{max h}$)

$(\text{GeS}_2)_{1-x}(\text{Sb}_2\text{S}_3)_x, x$	$\langle CN \rangle / E^{03}$ (–eV)	F_{th} ($\text{W} \cdot \text{cm}^{-2}$)	h_{max} (nm)	$F_{max h}$ ($\text{W} \cdot \text{cm}^{-2}$)
● 0	2.66/2.97	–	–	–
● 0.08	2.63/2.86	66	100	188
● 0.18	2.60/2.77	31	515	161
●, □, ■ 0.34	2.54/2.46	4.2	730	106
● 0.51	2.50/2.31	1.5	180	34
● 0.70	2.45/2.06	n.d.	75	106
● 0.88	2.42/1.87	n.d.	80	51
■ $\text{Ge}_{0.18}\text{Sb}_{0.03}\text{S}_{0.79}$	2.39/2.78	87	180	161
■ $\text{Ge}_{0.19}\text{Sb}_{0.10}\text{S}_{0.71}$	2.48/2.62	8.0	700	78
□ $\text{Ge}_{0.13}\text{Sb}_{0.17}\text{S}_{0.70}$	2.43/2.54	9.2	630	133
□ $\text{Ge}_{0.16}\text{Sb}_{0.18}\text{S}_{0.66}$	2.50/2.51	17	410	106
□ $\text{Ge}_{0.24}\text{Sb}_{0.16}\text{S}_{0.60}$	2.64/1.96	21	40	133

The specific sets of glasses are denoted by the symbols ●, □, ■

n.d.—not determined; in the second column $\langle CN \rangle$ and E^{03} values are given for readers convenience

mean coordination number for the examined glasses. This parameter serves as an indicator of sample rigidity/flexibility and facilitates the comparison of glasses with varied chemical compositions. The mean coordination number ($\langle CN \rangle$) of each $\text{Ge}_x\text{Sb}_y\text{S}_z$ sample was calculated as $\langle CN \rangle = x \cdot N_{\text{Ge}} + y \cdot N_{\text{Sb}} + z \cdot N_{\text{S}}$, where the coordination numbers N_{Ge} , N_{Sb} and N_{S} are assumed to be 4, 3 and 2, respectively [44].

The dimensions of the fabricated microlenses, such as height and diameter, are crucial for their potential applications. They influence the microlenses' curvature radius and their effective focal length, in conjunction with the refractive index of the material/microlens [5].

The diameter of microlenses, as derived from our experiments, primarily depends on the laser beam diameter. Consequently, in our experiments, the microlenses diameter, $d_{\text{microlens}}$ was typically 40 μm or slightly lower, aligning well with the used laser beam diameter. The chemical composition of the sample did not significantly alter the microlenses' diameter.

In contrast, the heights of the microlenses under our tested conditions appear to correlate with the chemical composition, specifically through E^{03} . The maximum microlens heights (h_{max}) observed span a wide range, from tens to hundreds of nanometers, even when considering glasses with similar coefficients of thermal expansion (CTE, detailed for several stoichiometric glasses in the Supplementary materials, Table S1). For instance, a stoichiometric glass with $x = 0.88$

exhibited an h_{max} of just 80 nm and a CTE below T_g of approximately 12.1 ppm K^{-1} . In contrast, the glass with $x = 0.34$ presented an h_{max} of 730 nm and a CTE of about 11.3 ppm K^{-1} below T_g (refer to Table 2 and S1). Therefore, our findings suggest that the decisive factor determining the maximal height of microlenses, even among glasses with comparable CTE values, appears to be the E^{03} value, which ranged between 1.87 and 2.97 eV in our study.

In Fig. 5, we illustrate the relationship between h_{max} and the coordination number ($\langle CN \rangle$) of the examined glasses. It is evident that the $\langle CN \rangle$ values, which represent network rigidity, do not correlate with the observed h_{max} variations. Glasses with nearly identical $\langle CN \rangle$ values can exhibit markedly different h_{max} values. For instance, the stoichiometric glass with $x = 0.51$ and the sulphur-rich $\text{Ge}_{0.16}\text{Sb}_{0.18}\text{S}_{0.66}$ composition share the same $\langle CN \rangle$. Yet, the latter composition shows a h_{max} value that is more than double (approx. 410 nm compared to about 180 nm). The highest microlenses were observed for the stoichiometric glass with $x = 0.34$ ($h_{max} = 730$ nm, $\langle CN \rangle = 2.54$). Only marginally smaller was the h_{max} for the sulphur-rich non-stoichiometric $\text{Ge}_{0.19}\text{Sb}_{0.10}\text{S}_{0.71}$ glass, i.e. $h_{max} \approx 700$ nm, $\langle CN \rangle = 2.48$. Consequently, the influence of stoichiometry versus non-stoichiometry on h_{max} appears to be of minor significance in our observations, see Fig. 5, where there's no discernible trend in h_{max} concerning the stoichiometry or non-stoichiometry of the glasses.

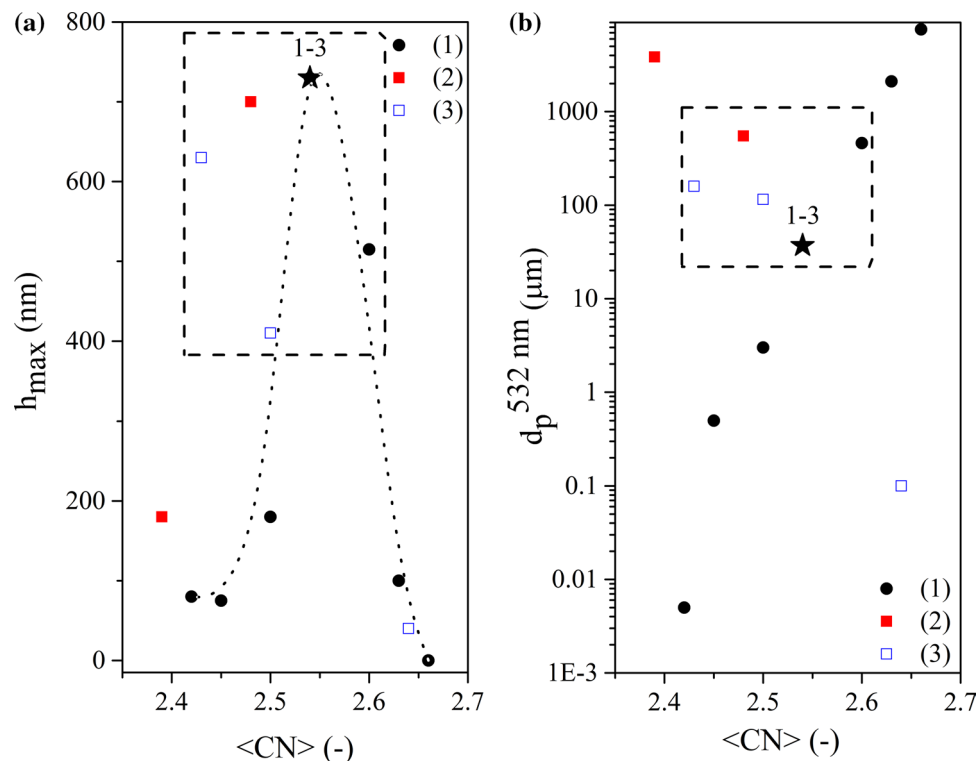


Figure 5 The dependency of **a** the maximal height of microlenses (h_{\max}) created on the surface of various Ge–Sb–S glasses and **b** the optical penetration depth of the used light ($d_p^{532\text{ nm}}$) on the coordination number (<CN>): (1) black circle—stoichiometric set of samples ($(\text{GeS}_2)_{1-x}(\text{Sb}_2\text{S}_3)_x$, $x=0\text{--}0.88$); (2)

red cube— $\text{Ge}_{0.18}\text{Sb}_x\text{S}_{0.82-x}$, $x=0.03\text{--}0.10$; (3) blue empty cube— $\text{Ge}_x\text{Sb}_{0.17}\text{S}_{0.83-x}$, $x=0.13\text{--}0.24$; black star (1–3)—composition shared across all three investigated sample series, i.e. $(\text{GeS}_2)_{0.66}(\text{Sb}_2\text{S}_3)_{0.34} \approx \text{Ge}_{0.18}\text{Sb}_{0.18}\text{S}_{0.64}$. The dotted line serves only as a guide for the eyes.

The dependences of h_{\max} on T_g and $d_p^{532\text{ nm}}$ values (see Table 1) were also analyzed. Initially, for the stoichiometric set of glasses, T_g values rise with increasing <CN> (indicating an increase of tetrahedral structural units), because both these parameters are associated with the strengthening/rigidity of the glassy network. However, h_{\max} displays a different trend in its dependence on <CN> when compared to the T_g versus <CN> relationship for stoichiometric samples. As depicted in Fig. 5a (black circles and black star), h_{\max} values ascend with a rise in <CN>, reaching a peak at <CN> = 2.54. Subsequently, however, as <CN> values continue to rise further, there's a pronounced decline in h_{\max} values.

The main parameter influencing the h_{\max} value in the examined Ge–Sb–S glasses appears to be optical penetration depth of the used light, denoted as $d_p^{532\text{ nm}}$. The volume of expandable material—contributing to microlenses' formation—is presumably determined by $d_p^{532\text{ nm}}$, given a constant laser beam diameter. It's worth mentioning that the actual depth employed for

the microlenses' formation might be slightly higher than the $d_p^{532\text{ nm}}$ value (equal to $1/\alpha^{532\text{ nm}}$), especially considering the lengthy exposition time of 600 s. The relationship between $d_p^{532\text{ nm}}$ and the peak microlenses height can be summarized as:

(a) Glasses with $h_{\max} < 200\text{ nm}$ exhibit two distinct $d_p^{532\text{ nm}}$ behaviors, potentially elucidating the observed responses to illumination in these materials. Certain glasses from this group have an E^{03} value (Table 1) significantly exceeding the energy of the employed photons ($E^{\text{ph}} = 2.33\text{ eV}$). This means sub-band gap photons undergo only minimal absorption. Consequently, the optical penetration depth of the light used significantly surpasses the material's thickness: $d_p^{532\text{ nm}} > 2.1\text{ mm}$, relative to $d_{\text{material}} \approx 1.4\text{ mm}$. An example is $(\text{GeS}_2)_{0.92}(\text{Sb}_2\text{S}_3)_{0.08}$ (<CN> = 2.63), which has a h_{\max} of merely 100 nm (as shown in Fig. 5). In such instances, the laser power density provided isn't potent enough to trigger notable photo-expansion throughout the material. The amount of absorbed energy is low and it disperses across the sample's entire thickness being

insufficient to cause significant thermal overheating and/or photo-structural changes. Therefore, the resulting microlenses are small, in this case ≈ 100 nm, see the h_{\max} values in Table 2 and Fig. 5.

For glasses where the E^{03} value is either comparable to or lower than E^{ph} (refer to Table 1 and Fig. 5), a similar behavior is evident. The $d_p^{532\text{ nm}}$ values are notably low, typically in the range of hundreds of nanometers or just a few micrometers. Consequently, the light employed is confined to a minuscule volume near the surface. As a result, photo-expansion is triggered only within this limited volume, leading to the formation of small microlenses with a maximum h_{\max} value of ≈ 200 nm.

(b) In contrast, the highest microlenses, exhibiting h_{\max} values ranging 410–730 nm under the given experimental conditions, were observed in glasses with $d_p^{532\text{ nm}}$ values spanning approx. 40–550 μm , see the dashed rectangles shown in both Fig. 5a, b. In these cases, the photon energy of the light used is between 0.84 and 0.95 of the E^{03} values. While this remains near sub-band gap light, its photon energy closely aligns with the band gap or E^{03} of the relevant glasses. Under such conditions, the light is predominantly absorbed in localized or defect states within the Urbach edge. Given the sample thickness and $d_p^{532\text{ nm}}$ value, a sufficient amount of energy is absorbed and transformed into volume expansion. This significant impact of near sub-band gap light on the height of the microlenses has also been noted in other chalcogenide glasses, e.g. As_2S_3 [11], Ge–As–S [45] or Ge–As–Se [46].

Moreover, we observed that the peak h_{\max} value ($x = 0.34$) for the stoichiometric set of glasses closely aligns with the highest probability of Ge–S–Sb linkages ($y = 60$, as denoted in Ref. [29], equating to 60 mol% of GeS_2 , in comparison to our glass containing 66 mol% of GeS_2). Notably, the highest microlenses on the surface of the Ge–As–S glassy system were detected in the $(\text{GeS}_2)_{0.59}(\text{As}_2\text{S}_3)_{0.41}$ composition [45]. This is analogous to our findings, as it essentially matches the highest likelihood of the proposed Ge–Ch–P linkages (where Ch represents chalcogen and P signifies pnictogen) as mentioned in [29]. Based on these results, we suppose that the unique structural characteristics of these compositions might influence microlenses formation and impact their maximal height.

Kutálek et al. [45] measured photo-induced expansion of Ge–As–S glass in-situ using thermomechanical analysis. They detected two forms of photo-expansion: temporary and permanent, where the temporary

expansion was observed only during the illumination, but after the illumination ceased, only the permanent expansion remained at the ambient temperature. We hypothesize that microlens formation primarily takes place above T_g , where viscous flow intensifies. Consequently, the transition time from the undercooled liquid to the glassy state during the cooling process may influence the balance between temporary and permanent volume shifts, thereby affecting the resultant microlens heights. Zallen [47] highlighted that eutectic compositions require the least time to transition from a melt to a glassy state during the cooling process. The composition with $x = 0.34$ is close to the eutectic point of the GeS_2 – Sb_2S_3 glassy system (see Ref. [5] in [29]). Thus, we suppose that the distinct cooling behavior of eutectic compositions might impact the balance between temporary and permanent photo-expansion, potentially explaining the maximum microlens height observed for glass with $x = 0.34$.

The threshold power density of microlenses formation (F_{th})

The threshold power density of microlenses formation (F_{th} , mentioned in Section "Direct laser writing by CW 532 nm laser") is another important parameter characterizing the creation of microlenses through illumination. This parameter denotes the maximum absorbed laser power density before the sample surface incurs damage/modification. Thus, to form microlenses, one must employ a laser power density exceeding the threshold power density.

The dependence of F_{th} value on $\langle\text{CN}\rangle$ for the examined glasses is illustrated in Fig. 6. For the binary GeS_2 glass ($\langle\text{CN}\rangle = 2.66$), microlenses formation was absent, attributable to the insufficient laser power density in tandem with the highest $d_p^{532\text{ nm}}$ and T_g among the glasses analyzed, as detailed in Table 1. For Sb_2S_3 rich glasses, i.e. $\langle\text{CN}\rangle = 2.42$ ($x = 0.88$) and 2.45 ($x = 0.70$), the heights of the microlenses were notably minimal, and we did not observe clear linear dependence on logarithm of laser power density (according to the Eq. (1) in Section "Direct laser writing by CW 532 nm laser"). Thus, under the experimental conditions applied to these compositions, determining the threshold power density was unfeasible.

The F_{th} values for the remaining samples are depicted in Fig. 6. In these cases, $\langle\text{CN}\rangle$ is not an appropriate parameter for correlating with F_{th} . Figure 6 illustrates distinct F_{th} versus $\langle\text{CN}\rangle$ relationships for

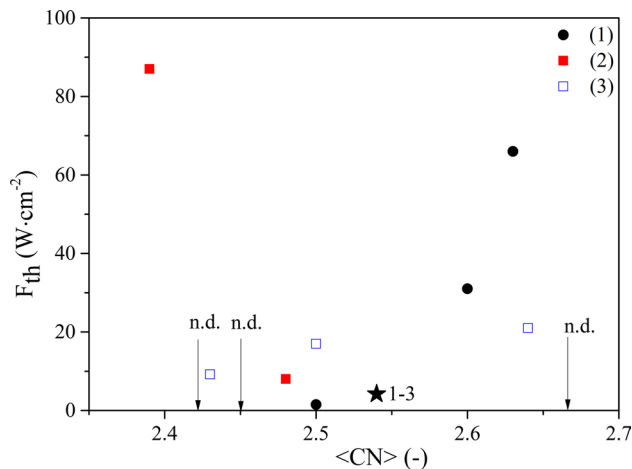


Figure 6 Correlation between the mean coordination number ($\langle CN \rangle$) and the threshold power density required for microlenses formation (F_{th}) for Ge–Sb–S glasses upon 532 nm illumination: (1) black circles—stoichiometric set of samples ($(GeS_2)_{1-x}(Sb_2S_3)_x$, $x=0–0.88$); (2) red cubes— $Ge_{0.18}Sb_xS_{0.82-x}$, $x=0.03–0.10$; (3) blue empty cube— $Ge_xSb_{0.17}S_{0.83-x}$, $x=0.13–0.24$; black star—sample composition/intersection of all three examined samples sets, i.e. $(GeS_2)_{0.66}(Sb_2S_3)_{0.34} \approx Ge_{0.18}Sb_{0.18}S_{0.64}$, n.d.—not determined, see text for detailed explanation.

each set of samples studied. Specifically, an upward trend of F_{th} in relation to an increase in $\langle CN \rangle$ was noted for the stoichiometric set of $(GeS_2)_{1-x}(Sb_2S_3)_x$ glasses, $x=0.08–0.51$. This contrasts with the varied behaviors observed for both non-stoichiometric sets, as shown in Fig. 6. We believe this discrepancy arises because the concept of $\langle CN \rangle$, derived from constraint theory [44, 48, 49], represents only the mechanical rigidity of the glassy network. However, this parameter does not consider binding energies and the roles of structural units. For example, a stoichiometric glass ($x=0.51$) favoring $SbS_{3/2}$ and $GeS_{4/2}$ structural units has a $\langle CN \rangle$ value of 2.50, identical to that of a sulfur-rich glass $Ge_{0.16}Sb_{0.18}S_{0.66}$, which is also expected to contain S–S bonds. Therefore, a meaningful correlation between F_{th} and $\langle CN \rangle$ is only evident when one type of structural unit is substituted for another, as mentioned above. Generally, the $\langle CN \rangle$ parameter was employed merely to simplify comparisons of glasses with varying Ge, Sb, and S compositions.

To explain the effect of chemical composition on the behavior of F_{th} , we employed the subsequent assumption: It is commonly accepted that the energy from absorbed photons elevates the sample's temperature, leading to the formation of microlenses due to the

localized thermal expansion of the overheated material. As a result, the optical and thermal properties of the examined glasses, including optical penetration depth, glass transition temperature, viscosity, thermal conductivity, and heat capacity, can significantly influence microlens formation. The roles of individual parameters can be described as follows:

- The glass transition temperature (T_g) is typically associated with the cross-linking and strengthening of the glass structure, which impacts surface modification. Moreover, the temperature-dependent viscosity of the resulting undercooled liquid also affects surface modification. Higher viscous flow, which facilitates surface shaping, is more evident above T_g .
- Our experiments indicate that the optical penetration depth ($d_p^{532\text{ nm}}$), given a consistent laser beam diameter, can serve as a parameter to estimate the extent of overheating during illumination, subsequently leading to the formation of microlenses.
- In our experiments, as a first approximation, we assumed that the heat capacity of the material (c_p) represents the amount of energy required to be locally absorbed to significantly overheat the illuminated volume of the material. As for thermal conductivity (κ), it can be said that it influences the rate of heat transfer and dissipation from the illuminated spot to its surroundings. Both parameters, therefore, influence the extent of overheating.

For stoichiometric samples, both parameters κ and c_p diminish as the $SbS_{3/2}$ structural units content increases, as detailed in Table S1 in the Supplementary materials. Concurrently, a rise in the $SbS_{3/2}$ structural units content results in a reduction of the optical penetration depth of the utilized light, coordination number, and glass transition temperature, as shown in Table 1 and 2. This trend aligns with the fragility behavior of undercooled liquids, which, when heated above T_g , also demonstrates an increase with the augmenting $SbS_{3/2}$ structural units content [32]. In other words, as temperature increase, the viscosity just above T_g alters more rapidly for Sb_2S_3 -rich glasses. In summary, the cumulative effect of these observations can account for the varying F_{th} values observed across the examined stoichiometric samples. For instance, the F_{th} value decreases with the decreasing $\langle CN \rangle$ value, corresponding to a rise in Sb_2S_3 content up to $x=0.51$.

For glass with $x = 0.51$, the minimal laser power density is required to trigger microlenses formation (Fig. 6 and Table 2), because a reduced volume of material (with a low $d_p^{532\text{ nm}}$) is required to adequately heat up to a relatively low T_g of the material. Additionally, a lesser quantum of energy absorption is needed to heat the sample, given that energy dissipation into the non-illuminated surroundings is also reduced, given the low values of c_p and κ in comparison to glasses with a higher GeS_2 concentration.

For Sb_2S_3 -rich glasses, while we couldn't determine the exact F_{th} value, microlenses were successfully created at relatively high F_L values $> 50\text{ W cm}^{-2}$ ($h_{max} < 100\text{ nm}$). In stoichiometric glass compositions, the influence of chemical composition on the laser power density required for microlens formation appears to have a non-monotonous trend, with the minimum F_{th} observed for a composition where $x = 0.51$. We hypothesize that the elevated F_L values needed for microlenses formation in Sb_2S_3 -rich glasses ($x = 0.70$ and 0.88) are primarily related to the $d_p^{532\text{ nm}}$ values, which are merely in order of tens or hundreds of nanometers (Table 1). In these glasses, light is predominantly absorbed within a small volume just beneath the surface. As a result, a portion of the generated heat might disperse across the glass surface-to-air interface, reducing local material overheating. This implies a greater F_L is required to achieve adequate overheating and subsequent local volume expansion or microlenses formation. Furthermore, a potential correlation may exist between the highest likelihood of Ge–S–Sb linkages and F_{th} , as both parameters show a similar reliance on the chemical composition in stoichiometric glass series [29].

Based on the results shown in Fig. 6 and Table 1, we assume that the combination of $d_p^{532\text{ nm}}$ and T_g

predominantly influences the values of F_{th} . Consequently, we tried to compare F_{th} values for some selected glasses from all three sets of Ge–Sb–S glasses in order to demonstrate the possible effect of T_g and $d_p^{532\text{ nm}}$ on F_{th} .

(a) As an example, we consider stoichiometric $(\text{GeS}_2)_{0.49}(\text{Sb}_2\text{S}_3)_{0.51}$ ($\langle CN \rangle = 2.50$, $d_p^{532\text{ nm}} \approx 3\text{ }\mu\text{m}$, $T_g = 265\text{ }^\circ\text{C}$), sulphur-rich $\text{Ge}_{0.18}\text{Sb}_{0.03}\text{S}_{0.79}$ ($\langle CN \rangle = 2.39$, $d_p^{532\text{ nm}} \approx 3.8\text{ }\mu\text{m}$, $T_g = 193\text{ }^\circ\text{C}$) and sulphur-poor $\text{Ge}_{0.24}\text{Sb}_{0.16}\text{S}_{0.60}$ ($\langle CN \rangle = 2.64$, $d_p^{532\text{ nm}} \approx < 0.1\text{ }\mu\text{m}$, $T_g = 327\text{ }^\circ\text{C}$) glasses and compare their F_{th} values with $d_p^{532\text{ nm}}$ and T_g (see Fig. 6 and also Table 3 for better clarity). It is clearly visible that all selected glasses differ in all $d_p^{532\text{ nm}}$, $\langle CN \rangle$ and T_g , see Table 3. The highest F_{th} value was observed for $\text{Ge}_{0.18}\text{Sb}_{0.03}\text{S}_{0.79}$ glass, i.e. $F_{th} \approx 87\text{ W cm}^{-2}$, despite its lowest T_g value. The reason for this behavior is high value of $d_p^{532\text{ nm}}$, which is significantly higher (≈ 2.7 times) than the thickness of the material. Thus, only a small part of used light is absorbed in the sample and a relatively high energy/laser power density has to be used to create a microlens.

The lowest F_{th} was determined for stoichiometric $(\text{GeS}_2)_{0.49}(\text{Sb}_2\text{S}_3)_{0.51}$, with values of $d_p^{532\text{ nm}}$ and T_g in the middle of the examined ranges (Table 3). Relatively high laser power densities ($F_{th} \approx 21\text{ W cm}^{-2}$) have to be applied to induce microlenses formation on the surface of sulphur-poor $\text{Ge}_{0.24}\text{Sb}_{0.16}\text{S}_{0.60}$ glass, probably due to a significantly higher T_g . In addition, in the case of $d_p^{532\text{ nm}}$, values are in order of only tens or hundreds of nanometers, the induced temperature rise may be partially mitigated by heat dissipation into the air, which could also contribute to a higher F_{th} for this glass.

(b and c) For glasses with comparable values of either T_g and $d_p^{532\text{ nm}}$, the second divergent parameter

Table 3 Demonstration of the effect of T_g and $d_p^{532\text{ nm}}$ on the values of F_{th} by comparison of selected Ge–Sb–S glasses: (a) glasses with different $\langle CN \rangle$, T_g , $d_p^{532\text{ nm}}$, (b) glasses with comparable $\langle CN \rangle$ and T_g , and (c) glasses with comparable value of $d_p^{532\text{ nm}}$

Composition	$\langle CN \rangle$ (–)	T_g ($^\circ\text{C}$)	$d_p^{532\text{ nm}}$ (μm)	F_{th} ($\text{W}\cdot\text{cm}^{-2}$)
<i>(a) Different values of each parameter ($\langle CN \rangle$, T_g, $d_p^{532\text{ nm}}$, F_{th})</i>				
$(\text{GeS}_2)_{0.49}(\text{Sb}_2\text{S}_3)_{0.51}$	2.50	265	3	1.5
$\text{Ge}_{0.18}\text{Sb}_{0.03}\text{S}_{0.79}$	2.39	193	3840	87
$\text{Ge}_{0.24}\text{Sb}_{0.16}\text{S}_{0.60}$	2.64	327	<0.1	21
<i>(b) Comparable $\langle CN \rangle$ and T_g</i>				
$(\text{GeS}_2)_{0.49}(\text{Sb}_2\text{S}_3)_{0.51}$	2.50	265	3	1.5
$\text{Ge}_{0.19}\text{Sb}_{0.10}\text{S}_{0.71}$	2.48	262	549	8.0
<i>(c) Comparable $d_p^{532\text{ nm}}$</i>				
$\text{Ge}_{0.19}\text{Sb}_{0.10}\text{S}_{0.71}$	2.48	262	549	8.0
$(\text{GeS}_2)_{0.82}(\text{Sb}_2\text{S}_3)_{0.18}$	2.60	366	461	31

appears to prevalently influence the value of F_{th} , e.g. $(\text{GeS}_2)_{0.49}(\text{Sb}_2\text{S}_3)_{0.51}$ and $\text{Ge}_{0.19}\text{Sb}_{0.10}\text{S}_{0.71}$ have practically the same value of $T_g \approx 265^\circ\text{C}$ and significantly differ in $d_p^{532\text{ nm}}$ ($\approx 3\ \mu\text{m}$ for $(\text{GeS}_2)_{0.49}(\text{Sb}_2\text{S}_3)_{0.51}$ versus $\approx 550\ \mu\text{m}$ for $\text{Ge}_{0.19}\text{Sb}_{0.10}\text{S}_{0.71}$), see Table 3. The different optical penetration depth therefore resulted in more than 5.3 times higher F_{th} value for glass with higher $d_p^{532\text{ nm}}$, i.e. for $\text{Ge}_{0.19}\text{Sb}_{0.10}\text{S}_{0.71}$. Likewise, for glasses with comparable $d_p^{532\text{ nm}}$ values, higher F_{th} values are typically observed for glasses with higher T_g , see e.g. results obtained for $\text{Ge}_{0.19}\text{Sb}_{0.10}\text{S}_{0.71}$ and $(\text{GeS}_2)_{0.82}(\text{Sb}_2\text{S}_3)_{0.18}$ in Table 3.

Based on the presented results, it is evident that glasses with greater optical penetration depth (d_p), particularly when $d_p > d_{\text{material}}$, and a high T_g tend to require a higher F_{th} value for microlenses formation. This implies that a higher laser power density is necessary to induce microlenses formation in such glasses. For glasses with similar values of these parameters, considering additional factors like κ , c_p , and the material structure can be useful.

Effective focal length of formed microlenses

Convex microlenses formed by illumination, often resulting from local photo-expansion of the illuminated material, are notably researched for their potential use in diverse optical and/or photonic devices. For such applications, a suitable characterization of the created microlenses is desirable, particularly regarding their effective focal length (f_e).

In Table 4, key parameters essential for the potential use of microlenses are detailed, including their height, diameter, full width at half maxima (FWHM), radius of curvature (R_c), and focal length (f_e). The parameters are specified for the highest microlenses developed on the surface of $(\text{GeS}_2)_{0.66}(\text{Sb}_2\text{S}_3)_{0.34}$ glass.

Table 4 Characteristics for selected microlenses formed on the surface of bulk $(\text{GeS}_2)_{0.66}(\text{Sb}_2\text{S}_3)_{0.34}$ glass: used laser power densities (F_L), microlenses height (h), diameter (D), full width at half maximum (FWHM), radius of curvature (R_c) and focal length (f_e)

F_L (W cm^{-2})	105	50	20
h (μm)	0.73	0.62	0.43
D (μm)	35.1	35.2	31.1
FWHM (μm)	11.4	12.1	10.1
R_c (μm)	210	250	280
f_e (μm)	145	170	190

The calculations of R_c and f_e were performed as in Ref. [5]. The linear refractive index of the glass (n_0) was estimated to be ≈ 2.47 for $(\text{GeS}_2)_{0.66}(\text{Sb}_2\text{S}_3)_{0.34}$ glass at $\lambda = 1064\ \text{nm}$, based on data presented by Petit et al. [22]. The height of the selected microlenses ranges from 0.43 to 0.73 μm , while their diameters lie between 31.1 and 35.2 μm . The full width at half maximum (FWHM) for these microlenses is confined to a narrow range of 10.1–12.1 μm . Notably, R_c values show minimal variation for the discussed microlenses, i.e. $\approx 210\ \mu\text{m}$ for the highest and 280 μm for the lowest microlens. A similar trend is evident for the effective focal lengths, with f_e values in the range ≈ 145 –190 μm (see Table 4). Therefore, these microlenses hold potential for device miniaturization, as their f_e values lie in the order of hundreds of micrometers.

Conclusion

This work focused on the microlenses formation on the surface of three sets of bulk Ge–Sb–S glasses by direct laser writing technique (CW laser with $\lambda = 532\ \text{nm}$). Using a combination of EDX analysis, Raman spectroscopy and Nanoindentation—coupled with our previous findings [45]—it appears that the formation of microlenses results from thermal overheating of the illuminated section of the material. According to our results, the chemical composition was identified as the primary factor influencing the formation and attributes of the microlenses (maximum achieved microlenses height (h_{max}) and threshold power density required to induce the microlenses formation (F_{th})). The value of h_{max} seems to be predominantly influenced by optical penetration depth of the used light ($d_p^{532\text{ nm}}$), with some contribution of the glassy structure given by its chemical composition. High microlenses (400–730 nm) were formed especially for glasses having $d_p^{532\text{ nm}}$ in order of tens or hundreds of micrometers. The highest microlenses ($h \approx 730\ \text{nm}$) were found on the stoichiometric glass with a composition of $(\text{GeS}_2)_{0.66}(\text{Sb}_2\text{S}_3)_{0.34}$. This can be attributed to its proximity to the eutectic in the GeS_2 – Sb_2S_3 system and the increased probability of Ge–S–Sb structural bonds.

The threshold power density values (F_{th}) for microlenses formation are primarily influenced by $d_p^{532\text{ nm}}$ and the glass transition temperature (T_g), with the glassy structure, largely determined by its chemical composition, also playing a role. While additional

thermal parameters, such as heat capacity and thermal conductivity, have potential impacts, their effects are difficult to assess since they interrelate and influence each other. Our results indicate that glasses with great $d_p^{532\text{ nm}}$ values (often matching or exceeding the sample's thickness) and elevated T_g values are likely to show higher F_{th} values, meaning more energy must be supplied to induce microlenses formation. The lowest F_{th} values are typically observed for glasses with $d_p^{532\text{ nm}}$ values in the range of single or tens of micrometers. Conversely, $d_p^{532\text{ nm}}$ values in the range of hundreds of nanometers or less may increase F_{th} , likely due to heat loss at the surface/air interface during illumination. In other words, the balance between the energy used (or the heat produced) and the heat lost to the surroundings can significantly influence the overheating of the illuminated region, and consequently, the threshold power density essential for microlenses formation induction.

Since the appropriate effective focal length of the formed microlenses is critically important, we note that under our experimental conditions, the highest microlenses formed on the $(\text{GeS}_2)_{0.66}(\text{Sb}_2\text{S}_3)_{0.34}$ glass surface showed effective focal length values of 145–190 μm .

Acknowledgements

Support from the Faculty of Chemical Technology, University of Pardubice (FChT UPa) is highly acknowledged by all authors. The authors thank for financial support from the grant of the Ministry of Education, Youth and Sports of Czech Republic (grant LM2023037). The authors would also like to thank for technical support to Ing. M. Caskova and Assoc. prof. P. Janíček (University of Pardubice, Faculty of Chemical Technology), for the language proofreading to Ing. F. Částek and for the measurements of nanoindentation to dr. J. Lukeš (ČVUT, Prague).

Author contributions

JS contributed to conceptualization, investigation, formal analysis, visualization, writing—original draft, writing—review & editing. PK contributed to conceptualization, investigation, supervision, visualization, funding acquisition, writing—original draft,

writing—review & editing. EČ, PK, ES, JS, JK, and LT helped in investigation and writing—review & editing.

Funding

Open access publishing supported by the National Technical Library in Prague.

Data availability

The datasets generated during the current study are available from the corresponding author on reasonable request.

Declarations

Conflict of interest The authors declare that there are no competing financial interests and also, they have no known competing financial interests or personal relationships that influence the work reported in this work.

Ethical approval Not applicable.

Supplementary Information The online version contains supplementary material available at <https://doi.org/10.1007/s10853-024-09353-6>.

Open Access This article is licensed under a Creative Commons Attribution 4.0 International License, which permits use, sharing, adaptation, distribution and reproduction in any medium or format, as long as you give appropriate credit to the original author(s) and the source, provide a link to the Creative Commons licence, and indicate if changes were made. The images or other third party material in this article are included in the article's Creative Commons licence, unless indicated otherwise in a credit line to the material. If material is not included in the article's Creative Commons licence and your intended use is not permitted by statutory regulation or exceeds the permitted use, you will need to obtain permission directly from the copyright holder. To view a copy of this licence, visit <http://creativecommons.org/licenses/by/4.0/>.

References

- [1] Mishra S, Yadava V (2015) Laser beam micromachining (LBMM): a review. *Opt Lasers Eng* 73:89. <https://doi.org/10.1016/j.optlaseng.2015.03.017>
- [2] Schaeffer R (2016) *Fundamentals of laser micromachining*. CRC Press, Boca Raton
- [3] Orava J, Kohoutek T, Greer AL, Fudouzi H (2011) Soft imprint lithography of a bulk chalcogenide glass. *Opt Mater Express* 1:796. <https://doi.org/10.1364/ome.1.000796>
- [4] Kasztelanec R, Kujawa I, Stepien R, Cimek J, Harasny K, Klimczak M, Waddie AJ, Taghizadeh MR, Buczynski R (2014) Fabrication and characterization of microlenses made of tellurite and heavy metal oxide glass developed with hot embossing technology. *Opt Quantum Electron* 46:541. <https://doi.org/10.1007/s11082-013-9811-0>
- [5] Sanchez EA, Waldmann M, Arnold CB (2011) Chalcogenide glass microlenses by inkjet printing. *Appl Opt* 50:1974. <https://doi.org/10.1364/ao.50.001974>
- [6] Zhang PC, Chen X, Yang H (2020) Large-scale fabrication of photonic nanojet array via template-assisted self-assembly. *Micromachines* 11:473. <https://doi.org/10.3390/mi11050473>
- [7] Loghina L, Palka K, Buzek J, Slang S, Vlcek M (2015) Selective wet etching of amorphous As_2Se_3 thin films. *J Non-Cryst Solids* 430:21. <https://doi.org/10.1016/j.jnoncrystol.2015.09.021>
- [8] Adam J, Zhang X (2014) *Chalcogenide glasses: preparation, properties and applications*. Woodhead Publishing, Cambridge
- [9] Tanaka K, Shimakawa K (2021) *Amorphous chalcogenide semiconductors and related materials*. Springer International Publishing, New York
- [10] Beadie G, Rabinovich WS, Sanghera J, Aggarwal I (1998) Fabrication of microlenses in bulk chalcogenide glass. *Opt Commun* 152:215. [https://doi.org/10.1016/S0030-4018\(98\)00172-2](https://doi.org/10.1016/S0030-4018(98)00172-2)
- [11] Hisakuni H, Tanaka K (1994) Giant photoexpansion in As_2S_3 glass. *Appl Phys Lett* 65:2925. <https://doi.org/10.1063/1.112533>
- [12] Chopra KL, Solomon Harshvardhan K, Rajagopalan S, Malhotra LK (1981) On the origin of photocontraction effect in amorphous chalcogenide films. *Solid State Commun* 40:387. [https://doi.org/10.1016/0038-1098\(81\)90844-9](https://doi.org/10.1016/0038-1098(81)90844-9)
- [13] Calvez L, Yang Z, Lucas P (2009) Reversible giant photocontraction in chalcogenide glass. *Opt Express* 17:18581. <https://doi.org/10.1364/oe.17.018581>
- [14] Kutálek P, Knotek P, Šandová A, Vaculovič T, Černošková E, Tichý L (2021) Ablation of binary As_2S_3 , As_2Se_3 , GeSe_2 , GeSe_3 bulk glasses and thin films with a deep ultraviolet nanosecond laser. *Appl Surf Sci* 554:149582. <https://doi.org/10.1016/j.apsusc.2021.149582>
- [15] Messaddeq SH, Dumont A, Douaud A, El-Amraoui M, Messaddeq Y (2018) Formation of cross-superposed LIPSSs on bulk chalcogenide glasses using fs-laser. *Adv Opt Technol* 7:311. <https://doi.org/10.1515/aot-2018-0031>
- [16] Deng H, Qi D, Wang X, Liu Y, Shangguan S, Zhang J, Shen X, Liu X, Wang J, Zheng H (2023) Femtosecond laser writing of infrared microlens arrays on chalcogenide glass. *Opt Laser Technol* 159:108953. <https://doi.org/10.1016/j.optlastec.2022.108953>
- [17] Zhou W, Li R, Qi Q, Yang Y, Wang X, Dai S, Song B, Xu T, Zhang P (2022) Fabrication of Fresnel zone plate in chalcogenide glass and fiber end with femtosecond laser direct writing. *Infrared Phys Technol* 120:104004. <https://doi.org/10.1016/j.infrared.2021.104004>
- [18] Hisakuni H, Tanaka K (1995) Optical fabrication of microlenses in chalcogenide glasses. *Opt Lett* 20:958. <https://doi.org/10.1364/ol.20.000958>
- [19] Frumar M, Tichá H, Bureš M, Koudelka L (1975) Semi-conducting glass of system Ge–Sb–S. *Z Chem* 15:199
- [20] Linke D, Böckel I (1976) Eigenschafts-korrelationen bei chalcogenidgläsern. I. Das system germanium-antimon-schwefel. *Z Anorg Allg Chem* 419:97
- [21] Bletskan D (2006) Glass formation in binary and ternary chalcogenide systems. *Chalcogenide Lett* 3:81
- [22] Petit L, Carlie N, Adamietz F, Couzi M, Rodriguez V, Richardson KC (2006) Correlation between physical, optical and structural properties of sulfide glasses in the system Ge–Sb–S. *Mater Chem Phys* 97:64. <https://doi.org/10.1016/j.matchemphys.2005.07.056>
- [23] Takebe H, Hirakawa T, Ichiki T, Morinaga K (2003) Thermal stability and structure of Ge–Sb–S glasses. *J Ceram Soc Jpn* 111:572. <https://doi.org/10.2109/jcersj.111.572>
- [24] El-Hamalawy AA, El-Zaidia MM, Ammar AA, Elkholy MM (1994) Density, differential thermal analysis and direct-current conductivity of $\text{Sb}_{10}\text{S}_{90-x}\text{Ge}_x$ chalcogenide glasses. *J Mater Sci Mater Electron* 5:147
- [25] Koudelka L, Frumar M, Pisárčik M (1980) Raman spectra of Ge–Sb–S system glasses in the S-rich region. *J Non-Cryst Solids* 41:171. [https://doi.org/10.1016/0022-3093\(80\)90162-3](https://doi.org/10.1016/0022-3093(80)90162-3)
- [26] Koudelka L, Horák J, Pisárčik M (1981) Raman spectra of the $(\text{GeS}_2)_{1-x}(\text{Sb}_2\text{S}_3)_x$ system glasses. *Chem Zvesti* 35:327
- [27] Pethes I, Nazabal V, Ari J, Kaban I, Darpentigny J, Welter E, Gutowski O, Bureau B, Messaddeq Y, Jóvári P (2019) Atomic level structure of Ge–Sb–S glasses: chemical

- short range order and long Sb–S bonds. *J Alloy Compd* 774:1009. <https://doi.org/10.1016/j.jallcom.2018.09.334>
- [28] Lin C, Li Z, Ying L, Xu Y, Zhang P, Dai S, Xu T, Nie Q (2012) Network structure in $\text{GeS}_2\text{--Sb}_2\text{S}_3$ chalcogenide glasses: raman spectroscopy and phase transformation study. *J Phys Chem C* 116:5862. <https://doi.org/10.1021/jp208614j>
- [29] Tichy L, Ticha H (2015) On the “compositional threshold” in $\text{GeS}_2\text{--Sb}_2\text{S}_3$, $\text{GeSe}_2\text{--Sb}_2\text{Se}_3$ and $\text{GeS}_2\text{--Bi}_2\text{S}_3$ glasses. *Mater Chem Phys* 152:1. <https://doi.org/10.1016/j.matchemphys.2014.12.010>
- [30] Tichá H, Tichý L, Ryšavá N, Tříška A (1985) Some physical properties of the glassy $(\text{GeS}_2)_x(\text{Sb}_2\text{S}_3)_{1-x}$ system. *J Non-Cryst Solids* 74:37. [https://doi.org/10.1016/0022-3093\(85\)90398-9](https://doi.org/10.1016/0022-3093(85)90398-9)
- [31] Petit L, Carlie N, Richardson K, Humeau A, Cherukulapurath S, Boudebs G (2006) Nonlinear optical properties of glasses in the system Ge/Ga–Sb–S/Se. *Opt Lett* 31:1495. <https://doi.org/10.1364/ol.31.001495>
- [32] Shánělová J, Košťál P, Málek J (2006) Viscosity of $(\text{GeS}_2)_x(\text{Sb}_2\text{S}_3)_{1-x}$ supercooled melts. *J Non-Cryst Solids* 352:3952. <https://doi.org/10.1016/j.jnoncrysol.2006.06.026>
- [33] Knotek P, Tichy L (2012) On photo-expansion and microlens formation in $(\text{GeS}_2)_{0.74}(\text{Sb}_2\text{S}_3)_{0.26}$ chalcogenide glass. *Mater Res Bull* 47:4246. <https://doi.org/10.1016/j.materresbull.2012.09.024>
- [34] Knotek P, Tichy L (2013) Explosive boiling of $\text{Ge}_{35}\text{Sb}_{10}\text{S}_{55}$ glass induced by a CW laser. *Mater Res Bull* 48:3268. <https://doi.org/10.1016/j.materresbull.2013.05.031>
- [35] Knotek P, Navesnik J, Cernohorsky T, Kincl M, Vlcek M, Tichy L (2015) Ablation of $(\text{GeS}_2)_{0.3}(\text{Sb}_2\text{S}_3)_{0.7}$ glass with an ultra-violet nano-second laser. *Mater Res Bull* 64:42. <https://doi.org/10.1016/j.materresbull.2014.12.027>
- [36] ISO, 4287:2000 (2000) Geometrical product specification (GPS). Surface texture. Profile method. Terms, definitions and surface texture parameters
- [37] Čermák P, Hejtmánek J, Plecháček T, Navrátil J, Kašparová J, Holý V, Zmrhalová Z, Jarošová M, Beneš L, Drašar Č (2019) Thermoelectric properties and stability of Tl-doped SnS. *J Alloy Compd* 811:151902. <https://doi.org/10.1016/j.jallcom.2019.151902>
- [38] Shuker R, Gammon RW (1970) Raman-scattering selection-rule breaking and the density of states in amorphous materials. *Phys Rev Lett* 25:222. <https://doi.org/10.1103/PhysRevLett.25.222>
- [39] Ben-Yakar A, Byer RL (2004) Femtosecond laser ablation properties of borosilicate glass. *J Appl Phys* 96:5316. <https://doi.org/10.1063/1.1787145>
- [40] Smolík J, Knotek P, Schwarz J, Černošková E, Janíček P, Melánová K, Zárbybnická L, Pouzar M, Kutálek P, Staněk J, Edlman J, Tichý L (2022) 3D micro-structuring by CW direct laser writing on $\text{PbO--Bi}_2\text{O}_3\text{--Ga}_2\text{O}_3$ glass. *Appl Surf Sci* 589:152993. <https://doi.org/10.1016/j.apsusc.2022.152993>
- [41] Messaddeq S-H, Mastelaro V, Li M, Tabackniks M, Lezal D, Ramos A, Messaddeq Y (2003) The influence of oxygen in the photoexpansion of GaGeS glasses. *Appl Surf Sci* 205:143. [https://doi.org/10.1016/s0169-4332\(02\)01013-9](https://doi.org/10.1016/s0169-4332(02)01013-9)
- [42] Oliver WC, Pharr GM (2004) Measurement of hardness and elastic modulus by instrumented indentation: advances in understanding and refinements to methodology. *J Mater Res* 19:3. <https://doi.org/10.1557/jmr.2004.19.1.3>
- [43] Smolík J, Knotek P, Schwarz J, Černošková E, Kutálek P, Králová V, Tichý L (2021) Laser direct writing into $\text{PbO--Ga}_2\text{O}_3$ glassy system: parameters influencing microlenses formation. *Appl Surf Sci* 540:148368. <https://doi.org/10.1016/j.apsusc.2020.148368>
- [44] Phillips JC (1979) Topology of covalent non-crystalline solids I: short-range order in chalcogenide alloys. *J Non-Cryst Solids* 34:153. [https://doi.org/10.1016/0022-3093\(79\)90033-4](https://doi.org/10.1016/0022-3093(79)90033-4)
- [45] Kutálek P, Samsonova E, Smolík J, Knotek P, Schwarz J, Černošková E, Janíček P, Tichý L (2023) Microlenses formation on surface of stoichiometric Ge–As–S bulk glasses by CW laser direct writing. *Appl Surf Sci* 628:157380. <https://doi.org/10.1016/j.apsusc.2023.157380>
- [46] Calvez L, Yang Z, Lucas P (2008) Light-induced matrix softening of Ge–As–Se network glasses. *Phys Rev Lett* 101:177402. <https://doi.org/10.1103/PhysRevLett.101.177402>
- [47] Zallen R (1983) The physics of amorphous solids. John Wiley & Sons, New York
- [48] Phillips JC (1981) Topology of covalent non-crystalline solids II: medium-range order in chalcogenide alloys and A–Si(Ge). *J Non-Cryst Solids* 43:37. [https://doi.org/10.1016/0022-3093\(81\)90172-1](https://doi.org/10.1016/0022-3093(81)90172-1)
- [49] Thorpe MF (1983) Continuous deformations in random networks. *J Non-Cryst Solids* 57:355. [https://doi.org/10.1016/0022-3093\(83\)90424-6](https://doi.org/10.1016/0022-3093(83)90424-6)

Publisher’s Note Springer Nature remains neutral with regard to jurisdictional claims in published maps and institutional affiliations.